

Fully-resolved array of simulations investigating the influence of the magnetic Prandtl number on MHD turbulence

Mairi E. McKay,* Arjun Berera,† and Richard D.J.G. Ho‡

School of Physics and Astronomy, University of Edinburgh,

James Clerk Maxwell Building, Peter Guthrie Tait Road, Edinburgh, EH9 3FD, Scotland

(Dated: January 16, 2019)

We explore the effect of the magnetic Prandtl number Pm on energy and dissipation in fully-resolved direct numerical simulations of steady-state, mechanically-forced homogeneous magneto-hydrodynamic turbulence in the range $1/32 < Pm < 32$. We compare the spectra and show that if the simulations are not fully resolved, the steepness of the scaling of the kinetic-to-magnetic dissipation ratio with Pm is overestimated. We also present results of decaying turbulence with helical and nonhelical magnetic fields, where we find nonhelical reverse spectral transfer for $Pm < 1$ for the first time. The results of this systematic analysis have applications ranging from stars, planetary dynamos, and accretion disks.

I. INTRODUCTION

Turbulence is observed in an enormous variety of situations but fully understood in few. When an electrically-conducting fluid is exposed to a magnetic field, the turbulent dynamics can be described by the magnetohydrodynamic (MHD) equations, which dictate how the two main aspects of the fluid (the velocity and magnetic fields) interact. The seminal work on MHD was done by Hannes Alfvén [1], earning him the Nobel Prize. MHD offers valuable insights into astrophysical and geophysical phenomena, including the solar wind and the Earth’s magnetic field, and aids the development of industrial processes such as fusion reactors [2–6].

Physical properties of a magnetofluid affect its behaviour. One such property is the magnetic Prandtl number $Pm = \nu/\eta$, where ν is the kinematic viscosity and η the magnetic resistivity, which is a material property of the fluid. We may also write $Pm = Rm/Re$, where Rm and Re are the magnetic and kinetic Reynolds numbers, quantifying respectively the turbulence of the magnetic and kinetic components of the fluid. In nature, extreme values of Pm are commonplace: stellar and planetary interiors are in the range $Pm \sim 10^{-4}$ to 10^{-7} and smaller, while the interstellar medium and cosmological-scale magnetic fields have estimated values of $Pm \sim 10^{10}$ to 10^{14} [5, 7–11]. The achievable range of Pm in direct numerical simulations (DNS) is highly restricted because of computational requirements and is often set to one, which is not representative of most magnetofluids. Extrapolating from simulations with Pm in the vicinity of one is often necessary when connecting computational results to real-life applications. That said, the region around unity is not without its applications: black hole accretion disk models indicate that Pm may transition from being very small in most of the disk, to being greater

than one near the centre, which may explain the change of state from emission to accretion in these objects [12]. Estimates of Pm in the solar wind and solar convective zone are $Pm \simeq 1$ [5, 13].

In this paper we present an array of 36 high-resolution DNS of mechanically-forced, homogeneous, incompressible magnetohydrodynamic turbulence without a mean magnetic field, with $1/32 < Pm < 32$. Additionally, we present 18 decaying simulations with $1/16 < Pm < 16$, in which we test the effect of Pm on reverse spectral energy transfer (which includes any transfer of energy from small to large scales is not restricted to just inverse cascade). With our forced data we focus on the energy spectra, the ratios of the total kinetic and magnetic energies E_K/E_M , called the Alfvén ratio, and the kinetic and magnetic dissipation rates $\varepsilon_K/\varepsilon_M$. We also discuss resolution requirements in connection with recent theoretical findings.

In previous studies, an approximate scaling $\varepsilon_K/\varepsilon_M \simeq Pm^q$ was found [14, 15]. The parameter q varied depending on the magnetic helicity (which includes the knottedness of the magnetic field, and contributions from twist, writhe, and linkage [16, 17]) and whether Pm was greater than or less than one. However, these papers only guaranteed full resolution of one dissipation scale. In other words, the largest wavenumber in the simulation, k_{max} , was greater than either the kinetic dissipation wavenumber $k_\nu = (\varepsilon_K/\nu^3)^{1/4}$ or the magnetic dissipation wavenumber $k_\eta = (\varepsilon_M/\eta^3)^{1/4}$, but not both. This is an issue because although a system’s energy is mostly concentrated in the largest length scales, the dissipation spectrum is proportional to the wavenumber squared. In hydrodynamic turbulence, in order to capture 99.5% of the dissipative dynamics, the condition $k_{max} > 1.25k_\nu$ must be fulfilled [18–20]. This was our definition of ‘fully-resolved’ and in all our forced simulations we had both $1.25k_\nu < k_{max}$ and $1.25k_\eta < k_{max}$. This paper also gives an explanation for the scaling which has not been done before.

Our set of forced simulations are an extensive dataset for DNS of homogeneous MHD turbulence, with 36 data points in the Re - Rm plane covering a square grid (see

* mairi.mckay@ed.ac.uk

† ab@ph.ed.ac.uk

‡ richard.ho@ed.ac.uk

Fig. 1). Re and Rm range from approximately 50 to 2300, allowing for a three order of magnitude range in magnetic Prandtl number. Each point was run on a 512^3 or 1024^3 lattice depending on individual resolution requirements, ensuring all data was fully resolved. This is the largest fully-resolved dataset for a Pm study.

Large values of magnetic helicity encourage reverse spectral transfer (RST), where energy is transferred to the largest length scales in the system, rather than to the small, dissipative scales, as in the usual Richardson-Kolmogorov phenomenology [21–24]. Whilst RST does not imply an inverse cascade, an inverse cascade is a type of RST. The second aspect of our study covers magnetofluids with nonzero magnetic helicity. We found RST in both helical and nonhelical turbulence down to $\text{Pm} = 1/4$, increasing as Rm increased, with Re playing little role. We thus confirm the results of recent simulations that found RST without helicity [25–27] and have seminal results showing RST occurring for $\text{Pm} < 1$.

II. SIMULATIONS

We carried out DNS of the incompressible MHD equations

$$\partial_t \mathbf{u} = -\nabla P - (\mathbf{u} \cdot \nabla) \mathbf{u} + (\mathbf{b} \cdot \nabla) \mathbf{b} + \nu \nabla^2 \mathbf{u} + \mathbf{f}, \quad (1)$$

$$\partial_t \mathbf{b} = \nabla \times (\mathbf{u} \times \mathbf{b}) + \eta \nabla^2 \mathbf{b}, \quad (2)$$

$$\nabla \cdot \mathbf{u} = 0, \quad \nabla \cdot \mathbf{b} = 0, \quad (3)$$

where \mathbf{u} is the velocity field, \mathbf{b} is the magnetic field in Alfvén units, P is the total pressure, the density is constant and set to 1, and \mathbf{f} is a random force defined via a helical basis:

$$\mathbf{f}(\mathbf{k}, t) = A(\mathbf{k}) \mathbf{e}_1(\mathbf{k}, t) + B(\mathbf{k}) \mathbf{e}_2(\mathbf{k}, t), \quad (4)$$

where $\mathbf{e}_1 \cdot \mathbf{e}_2^* = \mathbf{e}_1 \cdot \mathbf{k} = \mathbf{e}_2 \cdot \mathbf{k} = 0$ and \mathbf{e}_1 and \mathbf{e}_2 are unit vectors satisfying $i\mathbf{k} \times \mathbf{e}_1 = k\mathbf{e}_1$ and $i\mathbf{k} \times \mathbf{e}_2 = -k\mathbf{e}_2$ [28–30]. $A(\mathbf{k})$ and $B(\mathbf{k})$ are variable parameters that allow the injection of helicity to be adjusted; we chose to force nonhelically. We solved the MHD equations numerically using a pseudospectral, fully-dealiased code (see [18, 31] for details) on a three-dimensional periodic domain. The initial fields were random Gaussian with magnetic and kinetic energy spectra of the form $E_{M,K}(k, t=0) = Ck^4 \exp(-k^2/(2k_0)^2)$, where C is a positive real number and k_0 is the peak of the spectrum. In our forced simulations we set $k_0 = 5$ and forced the velocity field at the largest scales, $1 \leq k \leq 2.5$. The nature of the forcing function and the forcing length scale do not greatly affect the dynamics [28, 32]. We also ran decaying simulations, where we were less interested in the inertial range energy spectra and more interested in RST, so we set the peak at $k_0 = 40$. There was no imposed magnetic guide field. The viscosity and resistivity of each simulation are given in Fig. 1; note that $\text{Rm} \simeq 0.65/\eta$ and $\text{Re} \simeq 0.65/\nu$. This value of 0.65 comes from the fact that

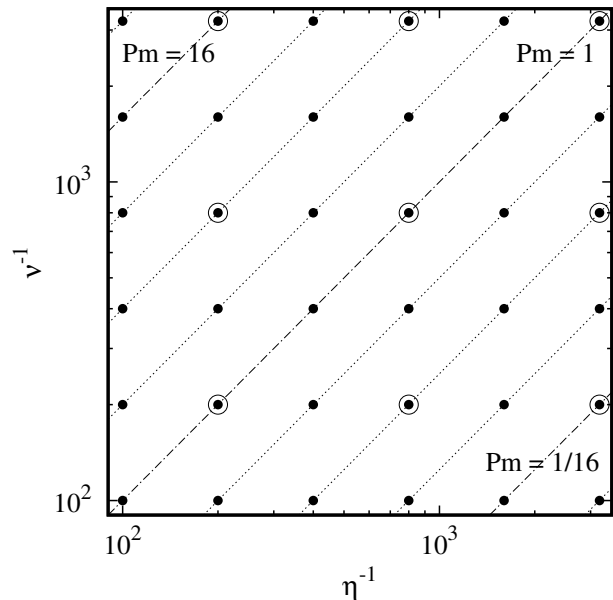


FIG. 1: Small circles show ν^{-1} and η^{-1} for each of the 36 simulations appearing in Figs. 2, 3 and 4. The 9 large circles indicate the decaying helical and nonhelical simulations with initial spectra peaking at $k_0 = 40$ (see Fig. 6). The lines indicate points of constant $\text{Pm} = 2^n$ for $-5 \leq n \leq 5$. The largest and smallest values of η and ν are 0.01 and 0.0003125.

the rms velocity u and integral length scale L are relatively constant during the simulations, with $\text{Re} = uL/\nu$ and $\text{Rm} = uL/\eta$.

III. RESULTS

A. Energy

Figure 2a shows the time-averaged compensated kinetic energy spectra of selected simulations. In each of the three plots the solid line represents the same simulation, with $\text{Re}=\text{Rm} \simeq 2275$ and $\text{Pm} = 1$. The top plot shows the spectra of four simulations where Re and Rm were increased with $\text{Pm} = 1$ kept constant. The middle plot compares data with $\text{Rm} \simeq 2275$ and Pm increasing from 1 to 32 by decreasing Re; while the bottom plot shows data with $\text{Re} \simeq 2275$ and Pm being decreased from 1 to $1/32$ via decreasing Rm. When we increase Re but keep Pm constant, as in the top plot, we see that less energy is stored in the large scales of the velocity field, whereas if we increase Re but keep Rm constant and large-valued, as in the middle plot, the amount of energy in the large-scale velocity field is slightly enhanced. The spectrum most closely resembling the Kolmogorov $k^{-5/3}$ scaling is the $\text{Pm} = 1/32$ run in the bottom plot, which seems to be below the dynamo action onset threshold,

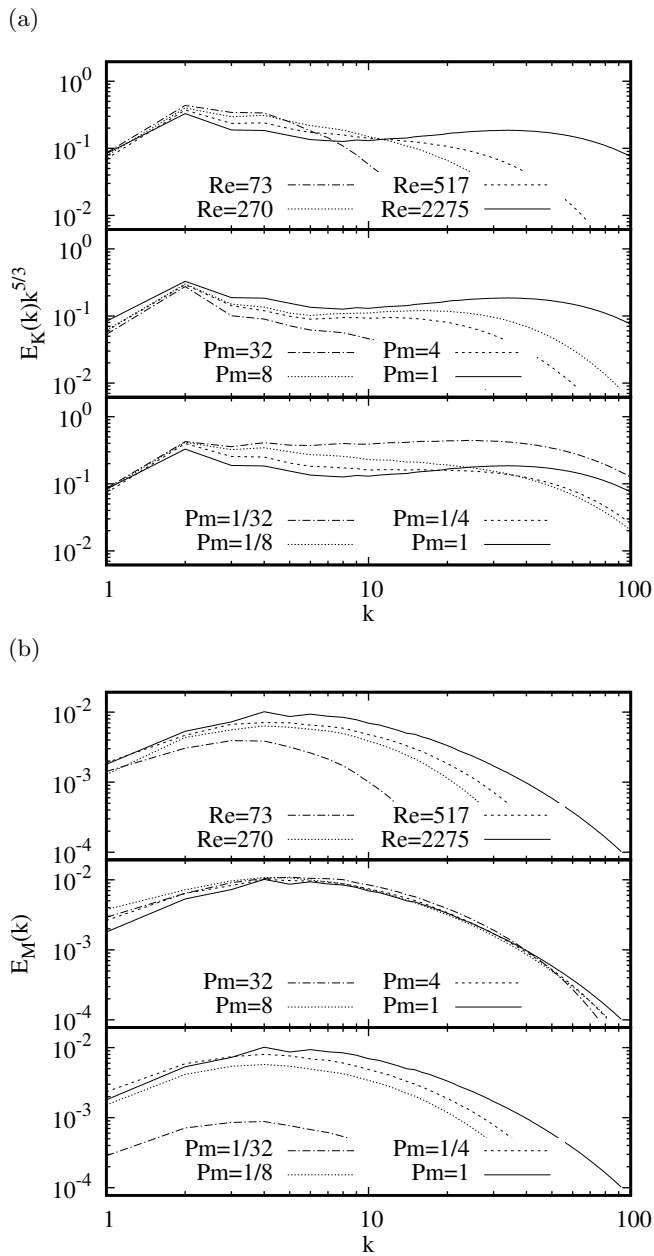


FIG. 2: Selected simulations, (a) shows kinetic energy spectra, compensated by $k^{-5/3}$, (b) shows uncompensated magnetic energy spectra. The top images show data with $Pm = 1$; the second show data with $Rm \simeq 2275$ and the third show $Re \simeq 2275$. In each plot the solid line corresponds to the same simulation, with $Pm = 1$ and $Re=Rm \simeq 2275$.

and so the magnetic field (which was initially in equipartition with the velocity field) will eventually decay completely, leaving a purely hydrodynamic simulation.

The corresponding magnetic energy spectra are shown in Fig. 2b. The spectra are most heavily influenced by Rm . In the top and bottom plots, Rm is varied while Pm and Re are respectively kept constant. The spectra pro-

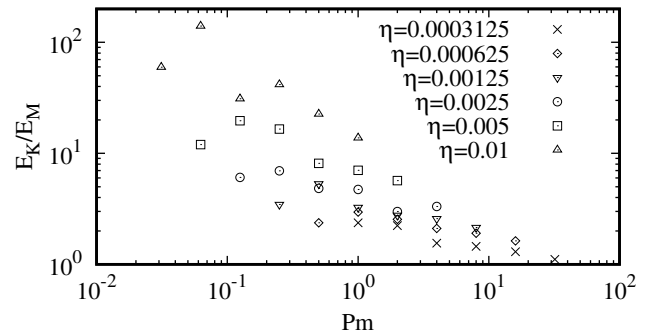


FIG. 3: Time-averaged Alfvén ratios of simulations grouped according to resistivity, η .

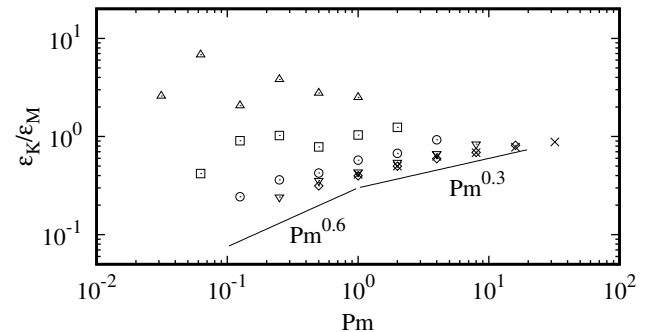


FIG. 4: Time-averaged kinetic-to-magnetic dissipation rate ratios grouped according to resistivity, η .

duced in these two plots are relatively similar except in the $Rm=73$ case, where for $Pm = 1$ the magnetic field is sustained but for $Pm = 1/32$ it is decaying. In the second plot we see that increasing Pm with constant Rm may slightly augment the large-scale magnetic field. Whilst this appears to imply Pm -dependence of the energy spectra, the total energy spectra $E_T(k) = E_K(k) + E_M(k)$ (equivalent to thinking in terms of Elsässer variables) appears to depend only on the maximum of Re or Rm , and is thus independent of Pm .

Figure 3 shows the time-averaged Alfvén ratios as a function of Pm , grouped into sets of points with approximately equal Rm . For fixed Rm the Alfvén ratios tend to decrease as Pm is increased, although the slope flattens at larger Rm . Bearing in mind that Rm doubles with each set of points, we see that the data are converging onto an asymptotic high- Rm limit. For all values of Pm , the ratio E_K/E_M decreases with increasing Rm . These behaviours are in agreement with what was put forward in Ref. [33].

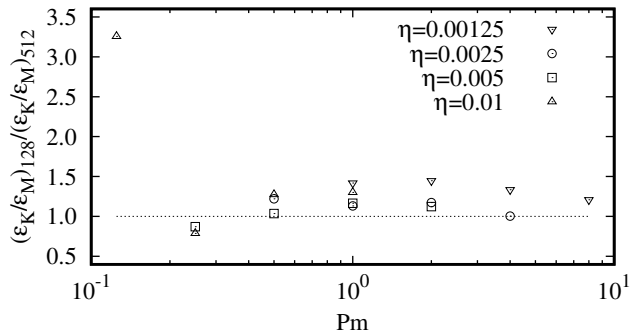


FIG. 5: Comparison of the time-averaged kinetic-to-magnetic dissipation rate in simulations on a 128^3 lattice $(\varepsilon_K/\varepsilon_M)_{128}$ and on a 512^3 lattice $(\varepsilon_K/\varepsilon_M)_{512}$ with otherwise identical initial conditions.

B. Dissipation

Figure 4 shows the kinetic-to-magnetic dissipation ratios for our dataset. Our $\text{Pm} > 1$ data collapse onto the same line as Rm increases, implying asymptotic independence from Rm when $\text{Pm} > 1$. The scalings for nonhelical MHD with $\text{Pm} < 1$ and $\text{Pm} > 1$ that were proposed in Ref. [14] have been indicated. Since for $\text{Pm} < 1$ the kinetic dissipation scale was not properly resolved in the simulations reported in Ref. [14], it is probable that the measurement of ε_K was affected, and similarly ε_M when $\text{Pm} > 1$, so the steepness of the scaling of $\varepsilon_K/\varepsilon_M$ with Pm appears exaggerated for both $\text{Pm} < 1$ and $\text{Pm} > 1$ compared to our results.

The total dissipation rate was controlled by the large-scale energy injection and is approximately constant across all of our simulations. In our mechanically-forced simulations ε_M is necessarily equal to the average net kinetic-to-magnetic energy transfer rate, so the ratio $\varepsilon_K/\varepsilon_M$ can be used as a measure of the efficiency of dynamo action. Smaller values mean more energy is being transferred to and dissipated via the magnetic field. The collapse of our data onto one line as Rm increases in Fig. 4 shows that there is a maximum dynamo efficiency which is curtailed as the magnetic Prandtl number increases; that is, although a magnetic field is more easily sustained at large values of Pm , it receives relatively less energy transfer from the velocity field. This is consistent with other work from a very different direction [34, 35] but within the same Pm range, that also supports a diminishing of the dynamo. At small values of Pm , ε_M may far exceed ε_K , meaning that if the kinetic-to-magnetic transfer rate is not able to match ε_M , any magnetic field will eventually dissipate fully. This line onto which the data collapses has an inflexion point about $\text{Pm}=1$, however, the equivalent line when plotting $\varepsilon_M/\varepsilon_T$ ($\varepsilon_T = \varepsilon_K + \varepsilon_M$) as a function of Pm shows no such inflexion. This serves as one explanation for the origin of the scaling behavior

of the dissipation ratio.

To illustrate the importance of resolution we repeated on a 128^3 lattice our simulations which had been done on a 512^3 lattice; see Fig. 5. The low-resolution simulations miscalculated the dissipation ratios by up to 40%, with the biggest discrepancies mostly occurring at high Rm . Additionally, for $\text{Pm} = 1/8$, where dynamo action was not sustainable, the low-resolution dissipation ratio was more than 3 times the high-resolution ratio.

Analyses of triad interactions and shell-to-shell energy transfers show that energy is transferred from the velocity field at the forcing scale to the magnetic and velocity fields at all scales in a way that depends on the separation between the giving and receiving scales and the energy contained in the involved scales, amongst other things [29, 36–40]. Therefore it is reasonable to expect a consistent scaling of $\varepsilon_K/\varepsilon_M$ with Pm that is not affected by whether $\text{Pm} < 1$ or $\text{Pm} > 1$, as we see in Fig. 4. Furthermore, when the velocity field is turbulent over a larger range of scales than the magnetic field, i.e. $k_\nu > k_\eta$ and $\text{Pm} < 1$, then for a given Rm there should be a corresponding value of Pm below which more energy will be transferred to the dissipative part of the magnetic field, $k > k_\eta$, than to $k < k_\eta$. It thus seems natural that the magnetic field would become unsustainable at some critical value of Pm , as put forward in Ref. [34]. The coupling between the small-scale velocity field and the large-scale magnetic field may be key to tipping the balance in favour of sustainable dynamo action for small values of Pm [41]. Indeed, this explains why the $\text{Pm} = 1/8$ result in Fig. 5 was so large: dynamo action in the low-resolution simulation was suppressed.

C. Reverse spectral transfer

In Fig. 2b the high- Rm data have more of a build-up of magnetic energy in the largest scales than the lower- Rm data. Inspired by this, we move on to examining the effect of Rm and Pm on RST by comparing simulations of decaying MHD turbulence with initially fully helical or nonhelical magnetic fields. We performed 9 pairs of simulations covering the range $1/16 \leq \text{Pm} \leq 16$ in multiples of 4, with the extreme values of ν and η being 0.005 and 0.0003125 (see Fig. 1). To facilitate RST, we set the peak of the initial energy spectra to $k_0 = 40$.

We define the energy in the first 3 wavenumbers of the magnetic field as $E_3(t) = \int_0^3 E_M(k, t) dk$. Since the system is not subject to an external force, then if $E_3(t)$ is constant or increasing, energy must be coming from smaller length scales. We measured $E_3(t)$ until the simulation entered a power law decay of total energy and plotted the results in Fig. 6. We found that increasing Pm by increasing Rm enhances the growth rate of RST, with a stronger effect than increasing Pm by decreasing Re . This indicates that RST should be possible as long as there is adequate separation of k_1 , k_0 and k_η , where $k_1 = 1$ is the largest wavenumber in the system and k_ν is

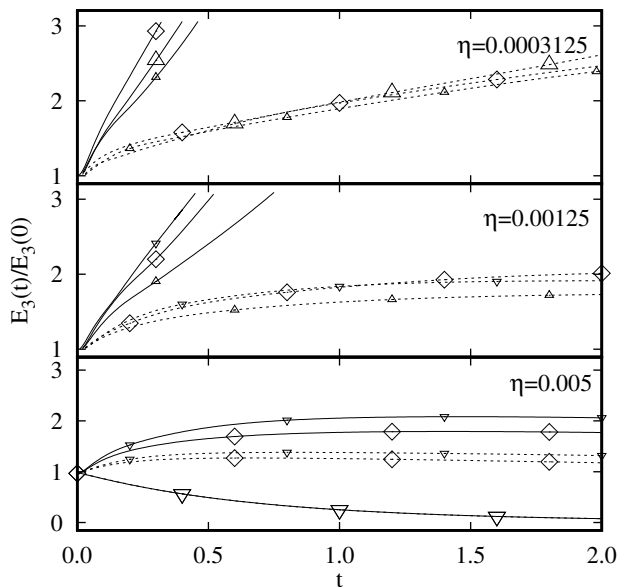


FIG. 6: $E_3(t)$ normalised by $E_3(0)$ for nonhelical runs (dashed lines) and helical runs (solid lines). Lines with diamond points correspond to $\text{Pr}_M = 1$, upwards-pointing small and large triangles to $\text{Pm} = 4$ and 16 , and downward-pointing small and large triangles to $\text{Pm} = 1/4$ and $\text{Pm} = 1/16$.

close to the value of k_η or greater. In general the high- Rm simulations (top plot in Fig. 6) had the most RST. RST was absent at $\text{Pm} = 1/16$ but present at $\text{Pm} = 1/4$ for high enough Rm . As far as we are aware, nonhelical RST for $\text{Pm} < 1$ has not been seen in previous DNS, and

may be of interest in geophysical applications [42].

IV. CONCLUSIONS

The fully-resolved simulations developed in this paper are a definitive dataset, improving confidence on the scaling and energy transfer properties of MHD in the near couple decade region of magnetic Prandtl number around unity. We have shown that many results rely on reaching a critical Rm before we find asymptotic dependence on Pm . Furthermore, underresolved simulations may exaggerate the scaling of properties such as $\varepsilon_K/\varepsilon_M$ by failing to account for all of the dissipative dynamics. Although our simulations feature simple geometry and do not take into account e.g. rotation, approaching complex physical problems from this angle may still have merit. In black hole accretion disks, luminosity is influenced by the dissipation ratios and DNS measurements could be a useful calibration tool. We reiterate that fully-resolved simulations such as ours are vital for accurately producing dynamo action and other effects incurred by nonunity Pm .

ACKNOWLEDGMENTS

This work used the ARCHER UK National Supercomputing Service [43], made available through the Edinburgh Compute and Data Facility (ECDF, [44]) and the Director's Time. AB acknowledges funding from the Science and Technology Facilities Council. MEM and RD-JGH were supported by the Engineering and Physical Sciences Research Council (EP/M506515/1). The data and simulation details are publicly available online [45].

-
- [1] H. Alfvén, *Nature* **150**, 405 (1942).
 - [2] D. Biskamp, *Magnetohydrodynamic Turbulence* (Cambridge University Press, Cambridge, UK, 2003).
 - [3] P. A. Davidson, *An Introduction to Magnetohydrodynamics* (Cambridge University Press, 2001).
 - [4] U. Frisch, *Turbulence: The Legacy of A. N. Kolmogorov* (Cambridge University Press, Cambridge, UK, 1995).
 - [5] M. K. Verma, *Physics Reports* **401**, 229 (2004).
 - [6] R. Keppens, J. P. Goedbloed, and J. W. S. Blokland, *Fusion Science and Technology* **57**, 137 (2010), <https://doi.org/10.13182/FST10-A9404>.
 - [7] C. Schrijver and G. Siscoe, *Heliophysics: Evolving Solar Activity and the Climates of Space and Earth* (Cambridge University Press, 2010).
 - [8] F. Plunian, R. Stepanov, and P. Frick, *Physics Reports* **523**, 1 (2013).
 - [9] C. Federrath, J. Schober, S. Bovino, and D. R. G. Schleicher, *Ap. J.* **797**, L19 (2014).
 - [10] J. Schober, D. Schleicher, and C. e. a. Federrath, *Ap. J.* **754**, 99 (2012).
 - [11] J. Schober, A. Brandenburg, I. Rogachevskii, and N. Kleeorin, “Magnetic prandtl number dependence of turbulence generated by chiral mhd dynamos,” (2018), arXiv:1803.06350 [physics.flu-dyn].
 - [12] S. A. Balbus and P. Henri, *The Astrophysical Journal* **674**, 408 (2008).
 - [13] M. K. Verma, *Journal of Geophysical Research: Space Physics* **101**, 27543 (1996).
 - [14] A. Brandenburg, *The Astrophysical Journal* **791**, 12 (2014).
 - [15] G. Sahoo, P. Perlekar, and R. Pandit, *New Journal of Physics* **13**, 013036 (2011).
 - [16] M. Berger and G. Field, *J. Fluid Mech.* **147**(1), 133 (1984).
 - [17] M. Berger, *Plasma Phys. Control. Fusion* **41**(1), B167 (1999).
 - [18] S. R. Yoffe, *Investigation of the transfer and dissipation of energy in isotropic turbulence*, Ph.D. thesis, The University of Edinburgh, Scotland (2012).
 - [19] D. A. Donzis, P. K. Yeung, and K. R. Sreenivasan, *Phys. Fluids* **20**, 045108 (2008).
 - [20] M. Wan, S. Oughton, S. Servidio, and W. H. Matthaeus, *Phys. Plasmas* **17**, 082308 (2010).

- [21] J. Léorat, U. Frisch, and A. Pouquet, *Annals of the New York Academy of Sciences* **257**, 173 (1975).
- [22] A. Pouquet, U. Frisch, and J. Léorat, *J. Fluid Mech.* **77**, 321 (1976).
- [23] A. Alexakis, P. D. Mininni, and A. Pouquet, *Astrophys. J.* **640**, 335 (2006).
- [24] A. Alexakis, P. D. Mininni, and A. Pouquet, *New Journal of Physics* **9**, 298 (2007).
- [25] A. Berera and M. Linkmann, *Phys. Rev. E* **90**, 041003 (2014).
- [26] A. Brandenburg and T. Kahniashvili, *Phys. Rev. Lett.* **118**, 055102 (2017).
- [27] A. Brandenburg, T. Kahniashvili, and A. G. Tevzadze, *Phys. Rev. Lett.* **114**, 075001 (2015).
- [28] M. E. McKay, M. Linkmann, D. Clark, A. A. Chalupa, and A. Berera, *Phys. Rev. Fluids* **2**, 114604 (2017).
- [29] F. Waleffe, *Phys. Fluids A* **4**, 350 (1992).
- [30] M. Lesieur, *Turbulence in fields* (Nijhoff, Boston, MA, 1987).
- [31] M. F. Linkmann, *Self-organisation processes in (magneto)hydrodynamic turbulence*, Ph.D. thesis, The University of Edinburgh, Scotland (2016).
- [32] A. Brandenburg, N. E. L. Haugen, X.-Y. Li, and K. Subramanian, “Varying the forcing scale in low prandtl number dynamos,” (2018), arXiv:1805.01249 [physics.flu-dyn].
- [33] N. E. L. Haugen, A. Brandenburg, and W. Dobler, *The Astrophysical Journal Letters* **597**, L141 (2003).
- [34] A. A. Schekochihin, S. C. Cowley, J. L. Maron, and J. C. McWilliams, *Phys. Rev. Lett.* **92**, 054502 (2004).
- [35] Y. Ponty, P. D. Mininni, D. C. Montgomery, J. F. Pinton, H. Politano, and A. Pouquet, *Phys. Rev. Lett.* **94**, 164502 (2005).
- [36] M. Linkmann, A. Berera, M. McKay, and J. Jäger, *Journal of Fluid Mechanics* **791**, 61 (2016).
- [37] M. Linkmann, G. Sahoo, M. McKay, A. Berera, and L. Biferale, *The Astrophysical Journal* **836**, 26 (2017).
- [38] P. D. Mininni, *Ann. Rev. Fluid Mech.* **43**, 377 (2011), arXiv:1006.1817 [physics.flu-dyn].
- [39] A. Alexakis, P. D. Mininni, and A. Pouquet, *Phys. Rev. E* **72**, 046301 (2005).
- [40] R. Kumar, M. K. Verma, and R. Samtaney, *Journal of Turbulence* **16**, 1114 (2015), <https://doi.org/10.1080/14685248.2015.1057340>.
- [41] S. Boldyrev and F. Cattaneo, *Phys. Rev. Lett.* **92**, 144501 (2004).
- [42] P. D. Mininni, *Phys. Plasmas* **13**, 056502 (2006).
- [43] <http://www.archer.ac.uk/>.
- [44] <http://www.ecdf.ed.ac.uk>.
- [45] <http://dx.doi.org/10.7488/ds/2361>.